Simulation of the onset of the Southeast Asian monsoon during 1997 and 1998: The impact of surface processes

Yansen Wang, W. –K. Tao, K. –M. Lau and Peter J. Wetzel

Popular Summary

The onset of the southeast Asian monsoon during 1997 and 1998 was simulated with a coupled mesoscale atmospheric model (MM5) and a detailed land surface model. The rainfall results from the simulations were compared with observed satellite data from the TRMM (Tropical Rainfall Measuring Mission) TMI (TRMM Microwave Imager) and GPCP (Global Precipitation Climatology Project). The simulation with the land surface model captured basic signatures of the monsoon onset processes and associated rainfall statistics. The sensitivity tests indicated that land surface processes had a greater impact on the simulated rainfall results than that of a small sea surface temperature change during the onset period. In both the 1997 and 1998 cases, the simulations were significantly improved by including the land surface processes. The results indicated that land surface processes played an important role in modifying the low-level wind field over two major branches of the circulation; the southwest low-level flow over the Indo-China peninsula and the northern cold front intrusion from southern China. The surface sensible and latent heat exchange between the land and atmosphere modified the low-level temperature distribution and gradient, and therefore the low-level. The more realistic forcing of the sensible and latent heat from the detailed land surface model improved the monsoon rainfall and associated wind simulation.

Simulation of the onset of the Southeast Asian monsoon during 1997 and 1998: The impact of surface processes

Yansen Wang[1], W. –K. Tao[2], K. –M. Lau[2] and Peter J. Wetzel[2]

[1]*U.S. Army Research Laboratory, AMSRL-CI-EB*
[2]*Laboratory for Atmospheres*
NASA/Goddard Space Flight Center

Submitted to : J. Geophy. Res. (7/25/03)

Corresponding Author address: Dr. Y. Wang, U.S. Army Research Laboratory, ATTN: AMSRL-CI-EB, 2800 Powder Mill Road, Adelphi, MD 20783

Abstract

The onset of the southeast Asian monsoon during 1997 and 1998 was simulated with a coupled mesoscale atmospheric model (MM5) and a detailed land surface model. The rainfall results from the simulations were compared with observed satellite data from the TRMM (Tropical Rainfall Measuring Mission) TMI (TRMM Microwave Imager) and GPCP (Global Precipitation Climatology Project). The control simulation with the land surface model captured basic signatures of the monsoon onset processes and associated rainfall statistics. The sensitivity tests indicated that land surface processes had a greater impact on the simulated rainfall results than that of a small sea surface temperature change. In both the 1997 and 1998 cases, the simulations were significantly improved by including the land surface processes. The mechanism by which the land surface processes affect the moisture transport and the convection during the onset of the southeast Asian monsoon were analyzed. The results indicated that land surface processes played an important role in modifying the low-level wind field over two major branches of the circulation; the southwest low-level flow over the Indo-China peninsula and the northern cold front intrusion from southern China. The surface sensible and latent heat fluxes modified the low-level temperature distribution and gradient, and therefore the low-level wind due to the thermal wind effect. The more realistic forcing of the sensible and latent heat fluxes from the detailed land surface model improved the low-level wind simulation and associated moisture transport and convection.

1. Introduction.

The southeast Asian monsoon system dominates the regional large-scale atmospheric circulation and precipitation in April and May. The onset of the southeast Asian monsoon is signified by the sudden activation of convection over the South China Sea (SCS) and surrounding region in late April and early May (Tao and Chen, 1987; Lau and Yang, 1997). The convection jumps across the SCS in mid to late May to southern China and the northern part of the SCS (Lau and Yang, 1997). The prolonged precipitation in central and eastern China and Japan, namely the Meiyu and Baiyu rainy season, starts in June and marks the beginning of the east Asian monsoon. The next stage occurs when the rain belt jumps into the Huaihe river basin in July and northern and northeastern China in August. As the season progresses, the monsoon begins to withdraw southward quickly in August (Tao and Chen, 1987; Ding, 1992; 1994).

Although the southeast Asian monsoon system displays distinct annual regularity from onset to break and withdrawal, it is also characterized by pronounced inter-annual variability. This inter-annual variability is strongly influenced by large-scale climate phenomena such as the El Nino-Southern Oscillation (ENSO) (Meehl, 1987; Lau and Shen, 1992). On the other hand, the inter-annual variability is also related to regional-scale forcing such as the land surface conditions and snow cover (Barnett et al., 1989) and the thermal and mechanical effects of the topography and land-sea contrast (Ding, 1994). Due to the interaction of many different forces at various scales, numerical model simulation of the southeast Asian monsoon system is a challenging problem. General circulation model (GCM) simulations (Sperber et al., 1994; Samel et al., 1995; Lau and Yang, 1997; Liang and Wang; 1998) have shown reasonable capability in capturing large-scale climate features. However, due to their coarse resolution, they are incapable of simulating the mesoscale circulation in the monsoon system and associated precipitation. In recent studies, mesoscale models have been used to simulate heavy rain events in the southeast Asian monsoon over southern and central China. Wang et al. (2000) modeled the 1991 flood event associated with the monsoon over the Yangtze-Huai river valley using a mesoscale regional climate model. A torrential rain case associated with the Mei-Yu front during 1998 (Qian et al., 2003) and heavy precipitation events in Taiwan (Tao et al., 2003) were simulated successfully using MM5 coupled with a land surface model.

The focus of this paper is to study the mesoscale precipitation and circulation characteristics of the onset of the southeast Asian monsoon system. The surface processes, including both the land surface and ocean surface, have been emphasized in the model simulations. The mechanisms by which the land surface processes affect the moisture transport and the convection are discussed. The model simulation results are compared with satellite observations such as TRMM TMI (Kumerrow et al., 2001) and GCPC (Huffman et al., 1997) and from the South China Sea Monsoon Experiment (SCSMEX) (Lau and Li, 2002; Johnson and Ciesielski, 2003). The diagnostic water vapor budget and its sensitivity to the land and ocean surface treatment in the model are also analyzed.

2. Model and simulation design

The model system used in this study is a coupled Penn State/NCAR MM5 atmospheric model (Grell et al, 1994; Dudhia, 1993) and a land surface model, the Parameterization for Land-Atmosphere-Cloud Exchange (PLACE) (Wetzel and Boone, 1995). MM5 is a complete non-hydrostatic model. It employs reference pressure as the basis for a terrain following vertical coordinate and a fully compressible set of equations. It has various physics packages such as cumulus parameterization, radiation, boundary layer parameterization and cloud microphysics. In the non-hydrostatic formulation, various physics packages and grid-nesting features enable the model to simulate atmospheric processes at a convective scale. This model has evolved over the last two decades and has been tested on many different weather systems. The land surface model contains five soil layers for water and seven soil layers for temperature and includes options for 14 different soil and vegetation types. Model outputs include surface temperature, soil moisture, surface fluxes of sensible and latent heat, runoff, and other related hydrological parameters. PLACE was a participant in the Project for Inter-comparison of Land surface Parameterization Schemes (PILPS), and was demonstrated to be among the more stable, accurate models currently in existence (Chen et al., 1997). Recently, MM5 and PLACE have been coupled to produce a numerical modeling system to simulate the atmosphere and land surface processes more realistically (Lynn et al., 2001). The MM5-PLACE model has been tested under various land surface conditions with improved simulations. The critical reason for this success is that the PLACE model provides a more realistic surface sensible and latent heat fluxes.

The simulation domain for this study is shown in Fig.1. The nested grid ratio is 3:1 with a coarse-mesh grid resolution of 60 km and a fine-mesh grid resolution 20 km. The coarse-mesh covers most of Asia, and the fine-mesh covers the southeast Asian monsoon onset area including the Indo-China peninsula, the South China Sea, and southern China. The number of grid points (x, y, sigma) is 175 x 142 x 23 for the coarse-mesh domain and 175 x 142 x 23 in the fine-mesh domain. The simulation uses the Betts-Miller cumulus parameterization scheme (Betts, 1986), the Blackadar high-resolution planetary boundary layer scheme (Zhang and Anthes, 1982), and the microphysics and radiation schemes of Dudhia (1989). The coupled PLACE model (Wetzel and Boone, 1995) provided the surface fluxes and land surface processes for the simulation.

The MM5 model is initialized with interpolated of the $2.5^{\circ} \times 2.5^{\circ}$ resolution ECMWF TOGA (European Center for Medium Range Weather Forecast Tropical Ocean Global Atmosphere) reanalysis of wind, temperature and relative humidity at all mandatory pressure levels. The ECMWF TOGA reanalysis is also used for boundary conditions in the coarse-mesh domain. The PLACE model is initialized with the NCEP (National Center for Environmental Prediction) surface temperature and sea surface pressure reanalysis. Data from the International Satellite Land Surface Climatology Project (ISLSCP, Meeson et al., 1995) were used to obtain values of fractional vegetation cover and leaf area index, albedo, surface roughness, and soil type. The thermal conductivity and emissivity of the ISLSCP-provided types were derived from the values commonly available in the literature (Lynn et al., 2001).

The onset of the monsoon in two consecutive years, 1997 and 1998, was chosen for the simulations. The rainfall statistics and wind flow field was quite different according to the previous investigations (Lau et al., 1998; Johnson and Ciesielski, 2003). The onset of the 1997 southeast Asian monsoon was very strong and fast, while in 1998 itt was slower and weaker. The large-scale conditions were also very different. In 1997, the onset was during the early stages of the 1997 El Nino, while in 1998 the onset was at the start of 1998/1999 La Nina.

As part of the sensitivity tests for the land surface processes, the original slab (Grell et al., 1994) land surface model was applied. In slab model, the soil moisture was constant throughout the simulation while the soil temperature was updated according to a simple force-restore method. In the runs testing the effects of sea surface temperature (SST) on the onset processes, a constant SST was applied using the values at the model initialization time. The SST in other runs was updated every 12 hours using the NCEP global analysis data. For both 1997 and 1998 cases, three runs were made: a CONTROL run that included both the PLACE land model and a variable SST, a NOPLACE run with variable SST, but using the simpler SLAB model with fixed climatological soil moisture instead of PLACE, and a CSST run with PLACE included, but with SST held fixed at its initial value.

3. Results and analysis

3.1 Onset characteristics of the 1997 and 1998 monsoons

Fig. 2 shows the MM5-simulated 1997 daily-averaged wind at 850mb and rain rate (left column) from the CONTROL run versus the rainfall from the GPCP and wind from the ECMWF reanalysis (right column). For Brevity, the data from every three days during the 12-day simulations were plotted. The onset of the 1997 southeast Asian monsoon occurred from 19-21 May (Lau et al., 1998). Compared with the GPCP rainfall data (Huffman et al., 1997) and ECMWF wind analysis, the model simulation captured the wind and precipitation associated the onset. Although the GPCP data and ECMWF analysis have much coarser resolution (1 x 1 degree for GPCP, 2.5 x 2.5 for ECMWF) than the model simulation, the basic rainfall and wind distribution patterns from these data sets offer a good first order validation for the simulation. On May 18, the wind circulation in the SCS is controlled by a tropical high-pressure system, and very little rainfall is observed in the region. By May 20, the tropical high pressure system has pushed out of the SCS region completely, and strong westerly winds dominate the wind circulation. A strong convective rain band occurred between the 18-20^0 N latitude at the same time. The southeast wind from southeastern China combined with strong westerly winds from the Bay of Bengal to create a cyclonic vortex in the northern SCS. This vortex and the associated heavy precipitation is simulated well compared with the GPCP data. The vortex and associated rainfall stay in the SCS region for about seven days before moving gradually northwestward out of the simulation domain. In addition to the strong southwest wind from the Bay of Bangle, the strong southeast wind and the intermittent northern front from southern China play an important role during the onset period. Both the simulation and the ECMWF global analysis show that the northern branch flow nearly reached the central part of the SCS during the 24^{th} and 27^{th} of May.

Since the TRMM satellite began operating in late 1997, the 1998 simulation had higher resolution (0.5 x 0.5) data because of the TRMM TMI. Fig. 3 displays simulated rainfall and 850mb wind for CONTROL run (left column) and TMI-observed rainfall and the ECMWF 850mb wind (right column) every three days during the 12-day simulation. The empty "white areas" indicate where there is no TMI coverage. The daily rainfall rate was computed from the rain rates within the TMI covered tracks. Generally speaking, the 1998 simulation captured the basic rainfall pattern observed by the TRMM TMI. The heavy precipitation areas (>30 mm/day) agreed better with the observations than the light rain areas. The southeast wind circulation from the Bay of Bengle and Indo-China peninsula did not penetrate into the SCS as deep as shown in the ECMWF TOGA global analysis.

There are significant differences in the characteristics of the onset of the 1997 and 1998 southeast Asian monsoons. Westerly wind from the Bay of Bengal penetrated much faster, and the Pacific subtropical high retreated much faster from the SCS region during the 1997 onset. The NSCAT (NASA Scatterometer) derived surface winds for 1997 (Lau et al., 1998) and 1998 (Lau and Li, 2002) also showed a stronger westerly wind penetration into the SCS region in 1997. The 1998 onset period (15- 21 May) is longer than that in 1997 (19-21 May). The onset signals are also not as strong in the 1998. The differences in the characteristics between 1997 and 1998 may be related to the large-scale climate variability (Lau and Yang, 1997) such as ENSO. The onset of the 1997 southeast Asian monsoon was during the early stages of an ENSO year while in 1998 was at the complete end of the ENSO signal and the start of La Nina conditions.

3.2 Mean rainfall statistics and comparisons with satellite observation

The 1997 area averaged (10- 24 N, 108-123 E) mean precipitation rate is displayed as a time series in Fig. 4. The GPCP rainfall average for the same area is also plotted in the Fig. 4. The general temporal distribution of rainfall is simulated remarkably well compared with the GPCP data. The simulations, however, produce more rainfall than is estimated from the satellite, especially the simulation without the land surface model, NOPLACE. The spatial distribution of the simulated precipitation and GPCP data are shown in Fig. 5. The spatial distribution pattern basically agrees with the GPCP data, with high rainfall in the area of 8-11 N and 111-116 E. All of the simulations produced additional precipitation in the northern part of the SCS, which is not observed in the GPCP. Overall, the control simulation (with PLACE and variable SST) produced the best simulation compared with the GPCP data. The simulation without PLACE produced too much rainfall.

For the onset of the 1998 southeast Asia monsoon, both TRMM TMI and GPCP data are available for comparison. Fig. 6 shows the area-averaged time series of rainfall from the simulations and from the TMI and GPCP data. The rainfall estimates from the TMI and from the GPCP agree fairly well. The simulation results follow the basic trend of the satellite rainfall estimates, but the peak on 20 May is not well simulated. The spatial distributions of the rainfall during the simulation period are also plotted in Fig. 7. The simulations captured the precipitation bands along the northern and central parts of the SCS. However, the rainfall along the northern part of the Philippines is not well simulated. Again, the control simulation gives better simulation compared with the observations.

Generally speaking, the simulation of the 1997 onset is better than that for 1998. This is probably due to the onset signal being much stronger in the 1997. As indicated in section 3.1, the onset circulation pattern is also better simulated for 1997. The simulations for 1997 in general better predict the time of the onset compared to 1998. It is important to note that the simulation without PLACE produced too little rainfall in 1998 but produced too much rainfall in 1997 compared with the GPCP and TMI observations. The reason for this phenomenon will be explained in the following sections.

3.3 The water vapor budget over the SCS region

The water vapor budgets from the simulations offer a detailed quantitative description of the moisture sources and sinks during the onset period of the monsoon. They can identify the contributions from each facet of the control volumes and therefore the remote moisture source/sink versus the local moisture recycling. By comparing the water budgets from the various land and ocean surface treatments, their impact on the water budgets and precipitation can be clarified.

The dashed line in Fig. 1 shows the control volume where the water budgets are compared. To quantify the moisture processes, the regional-scale model's water budget was calculated by horizontally and vertically integrating the continuity equation for atmospheric moisture around a rectangular domain, which yields:

$$W=FW+FE+FS+FN+E-P+R \qquad (1)$$

where W is the total change of atmospheric water vapor which is generally a small term; FW, FE, FS, and FN are the vertically integrated moisture fluxes along the western, eastern, southern, and northern boundaries of the budget calculation domain, respectively; $Q=FW+FE+FS+FN$ is the total moisture convergence in the domain; E is the total surface evaporation, P is the total precipitation; and R is the residual term.

The area coincides with the SCSMEX (the South China Sea Monsoon Experiment) area and where the onset starts. Lau and Li (2002) used same area to compute the water budget from the SCSMEX analysis (Johnson and Ciesielski, 2003). The method for computing the water budget is similar to that shown in Bosilovich and Sun (1999) where the water fluxes are integrated in the model sigma coordinate on the each face of the control box. The water budgets for the various simulations are computed for both 1997 and 1998 (Fig. 8) using the data output from every hour. The general pattern for both the 1997 and 1998 onsets is similar. Most of the moisture comes from the western boundary of the domain, reflecting the strong southwesterly flow from the Bay of Bengal during the onset period (Lau et al., 1998). The second greatest contribution comes from the southern boundary of the domain. The evaporation/precipitation ratio is 45% and 60% for 1998 and 1997, respectively. The outflow of moisture for 1997 and 1998 is quite different. The greatest outflow of moisture is via the eastern boundary during 1997 and the northern boundary in 1998. These moisture flow patterns are very much related to the large-scale flow patterns during the 1997 and 1998 onset periods.

The land surface has a significant impact on the domain average moisture budgets (Fig. 9). There is a significant difference between the 1997 NOPLACE and CONTROL runs. In the CONTROL run (Fig. 8a), a small amount of moisture flows out of the control volume. However, there is a net influx of moisture in the NOPLACE run. This is due to modification of the northern frontal flow by the land surface processes. Similar effects are also seen between 1998 NOPLACE and CONTROL runs. The change in moisture influx from the western and northern boundaries was large. The mechanisms by which this occurs will be discussed in detail in the following two sections.

3.4 Land surface impact

The large-scale wind circulation can be broken down into two major branches during the southeast Asian monsoon onset period. One branch consists of a cold front over southern China which collides with southwesterly flow during the onset; the second branch is the strong southwesterly wind originating from the Bay of Bengal that flows over most of the Indo-China peninsula. Although these two branches of wind circulation are mainly controlled by large-scale forces, land surface processes do have a significant impact upon them at the mesoscale. The energy budget over the land surface and lower part atmosphere is determined by radiation as well as the latent and sensible heat flux exchange between the land surface and atmosphere. The ratio of the latent and sensible heat fluxes affects the depth of the boundary layer and the temperature distribution in the lower atmosphere. The magnitude of the circulation alteration is proportional to the horizontal temperature gradient and the depth in the atmosphere to which the temperature perturbation extends. The land surface modified temperature causes changes in the geostrophic wind with height, Z, as given by the thermal wind relationship (Holton, 1972):

$$\begin{aligned} \frac{\partial U_g}{\partial Z} &= -\frac{g}{fT}\frac{\partial T}{\partial y} \\ \frac{\partial V_g}{\partial Z} &= \frac{g}{fT}\frac{\partial T}{\partial x} \end{aligned} \qquad (2)$$

where U_g and V_g are the horizontal components of the geostrophic wind in the x and y directions. f is the Coriolis parameter, and T is the average temperature. The change in circulation alters the strength of the moisture flux into the region and the atmospheric stability which closely related to the convection.

The northern cold-front intrusion from southern China was very strong (see Fig. 2) in 1997 over the SCS. Although this branch of the flow does not bring a large amount of moisture, it does increase the sea surface evaporation once it arrives over the SCS by bringing colder temperatures over the relatively warmer sea surface. Land surface processes have a significant influence on this cold front by modulating of temperature via sensible heat flux. Fig. 10 displays the sensible fluxes averaged over the entire 1997 simulation period for the CONTROL and NOPLACE runs. The larger sensible heat fluxes in southeast China in the CONTROL run had the effect of diluting the cold front, thus the cold front in the NOPLACE run had stronger northerly wind penetration into the SCS compared with the CONTROL run (Fig. 11). The latent heat fluxes over land for the CONTROL run had slightly larger values than those in the NOPLACE run, however the latent heat fluxes over the ocean in the convectively disturbed area were greatly increased in the NOPLACE run (Fig. 12). This is due to deeper cold front penetration and enhanced convection and precipitation (Fig. 5) in the NOPLACE run. The colder air enhanced the sea surface evaporation. Stronger convection can also increase the intensity of the downdrafts, resulting in colder, drier surface air and therefore increase the ocean surface evaporation. This phenomenon has been observed and simulated in the tropical convective environment (Bradley et al., 1991; Young et al., 1992; Wang et al., 1996).

Land surface processes also modified the southwesterly flow from the Bay of Bengle significantly. The larger contrast in sensible heat fluxes between the ocean and the wester part of the Indo-China peninsula in both the 1997 (Fig. 10) and 1998 (Fig.14) CONTROL runs increased the strength of the southwest wind over the peninsula compared with the NOPLACE simulations (Figs. 13 and 15). The low-level flow from the southeast over Indo-China peninsula is especially more important for the 1998 case since the northern front from southern China is much weaker than in the 1997 case. The changes in the strength of the low-level flow caused significant differences in the moisture transport into the SCS region because the low-level flow has highest water vapor contents. The previous analysis of the water budget and the mean statistics are also in agreement with this argument.

The 1998 simulations produced more rainfall for the CONTROL run than the NOPLACE run. However, the 1997 CONTROL run produced much less rainfall than that of the NOPLACE run. The CONTROL run, which includes the detailed land surface model PLACE, produced better rainfall results in both the 1997 and 1998 simulations compared with the observations (see Figs 4 to 7) although the rainfall corrections due to the PLACE model had the opposite tendency. This is because the large-scale circulation, as analyzed above, was quite different during 1997 and 1998. The cold front from southern China was much stronger during the 1997 onset, while the southwest flow over the Indo-China peninsula was a more dominant factor in 1998. This also indicated that the PLACE model captured the spatial and temporal distribution of sensible and latent heat fluxes better than the simple, slab land surface model. The interaction of the large-scale circulations such as the depth of the cold front penetration and the strength of the southwest flow from the Bay of Bengal with the land surface processes are important for simulating the onset of the southeast Asia monsoon.

3.5 The effects of sea surface temperature variation

The variation in the treatment of SST (constant versus variable) during the simulation period had much less effect on precipitation and the water vapor budget than did the land surface. This conclusion is supported by the previous analysis of the mean precipitation statistics (Figs. 4 and 5) and water vapor budget (Figs. 8 and 9). The monsoon system in Southeast Asia is certainly related to the land-sea surface temperature contrast. However, the SST changes during the simulation period for 1997 and 1998 were not significant and so were not a dominant factor in the accurate simulation of the onset.

Fig. 16 shows the SST distribution from the NCEP global analysis during the onset periods for both 1997 and 1998. The data indicate that there was only a very small increase (less than a half degree) in the SST during the onset periods in both 1997 and 1998. This is probably due to the large percentage of deep cloud coverage and precipitation effects on the ocean surface. The small increase in SST is also reflected in the water budget analysis (Figs. 8 and 9), which shows a small increase in the latent heat fluxes over the SCS in both the control simulation. However, typically the SST shows a large jump according to the climatology data before the onset (He et al., 1992, Lau et al., 1998). It appears to be one of the dominant factors for the southeast Asian monsoon .

4. Summary and Conclusions

The coupled MM5-PLACE models were able to fairly well simulate the onset of the 1997 and 1998 southeast Asian monsoon onsets compared with TRMM TMI and GPCP rainfall data. The modeled circulation patterns during the monsoon onset periods agreed with other analyses which showed two branches of the circulation: one is the strong southwesterly winds over Indo-China and frontal flow from southern China, dominating the circulation. The onsets for 1997 and 1998 show significant variation. The rapid onset in 1997 may be related with the ENSO. The simulation results for 1997 are slightly better than for 1998 due to stronger large-scale forcing and onset signal.

Water budget analysis indicated that the main moisture source for convection in the SCS during the onset comes from the south and west (70%). Local sea surface evaporation contributed about 30% during this period. Moisture outflow along the northern and eastern boundaries depends on the strength of the wind circulation and the speed of the onset processes. There was a moisture outflow along the eastern boundary for the fast, strong onset in 1997 with small moisture inflow at the eastern boundary for the slow, intermittent onset in 1998.

The land surface processes have a significant influence on the mesoscale circulation and therefore the moisture influx and precipitation during the onset period. In both the 1997 and 1998 events, the simulation coupled with the PLACE model produced much better results than that using the simple, slab land surface model. The reason is that PLACE produces more realistic surface heat fluxes and better ratio betwenn the latent and sensible heat fluxes. The differential heat generated mesoscale circulation due to the land surface processes significantly modified the low-level wind circulation and therefore the moisture transport and frontal position. The 1997 simulation without PLACE produced much more rainfall compared with the observations because the model produced an unrealistic deep southward frontal intrusion. The 1998 simulation without

PLACE produced much less rainfall because the model produced a much weaker southwest circulation which brings most of the moisture from the Bay of Bengal. In both the 1997 and 1998 cases, the PLACE sensible heat fluxes over the coastal area of southern China and over Indo-China Peninsula has played a import role in producing better simulation results. SST has only a secondary effect on the precipitation when compared with the land surface processes. This is because there was very little change in SST during the simulated onsets periods.

Acknowledgements

This work was begun while the first author was working at NASA/Goddard Space Flight Center. The work is supported by the NASA headquarters Physical Climate Program and the NASA Tropical Rainfall Measurement Mission(TRMM). The authors are grateful to Dr. R. Kakar for his support of this research. We thank Steve Lang for correcting the English in the paper. Acknowledgement is also made to NASA Goddard Space Flight Center for computer time used for this research.

Figure Captions

Figure 1. Nested simulation domains. Domain1, the outer domain, has 175 x 142 x 23 grid points with a horizontal resolution of 60 km. Domain2, the inner domain, has 175 x 142 x 23 grid points with a horizontal resolution of 20 km. The dashed rectangle shows the area for the rainfall averages (Figs. 4 and 5) and the moisture budget analysis.

Figure 2. Simulated daily rainfall (mm/day) and 850mb wind (left column) during the 1997 onset; GPCP rainfall (mm/day) and 850mb wind from ECMWF TOGA global analysis (right column). The results are shown every three days.

Figure 3. Simulated daily rainfall (mm/day) and 850mb wind (left column) during the1998 onset; TRMM TMI rainfall (mm/day) and 850mb wind from ECMWF TOGA global analysis (right column). The results are shown every three days. The white areas on the TMI rainfall plots show where there is no orbital coverage for that day.

Figure 4. Time series of area averaged daily rainfall over the dash-line-enclosed rectangle (see Fig.1) for the 1997 simulations and GPCP data.

Figure 5. Average rainfall (mm/day) over simulation domain2 for 1997 for the CONTROL simulation, GPCP data, NOPLACE, and CSST.

Figure 6. Time series of area averaged daily rainfall over the dash-line-enclosed rectangle (see Fig.1) for the 1998 simulations and TRMM TMI and GPCP data.

Figure 7. Average rainfall (mm/day) over simulation domain2 for 1998 for the CONTROL run, TRMM TMI data, NOPLACE , and CSST runs.

Figure 8. Water vapor budget results integrated over the entire simulation period for the a) 1997 CONTROL simulation and b) 1998 CONTROL simulation. Note that vapor inflow into the control volume is positive, and outflow is negative. P=Precipitation; E=Evaporation from the surface; R=Residual; W=Total change in water vapor. Units are in $1 x 10^{13}$ kg/day.

Figure 9. Same as Figure 6 except for a) the NOPLACE simulation for 1997, b) the 1997 CSST simulation, c) NOPLACE simulation for 1998, and d) the 1998 CSST simulation.

Figure 10. Average sensible heat flux (w m^{-2}) simulated during the 1997 onset. The left panel is the CONTROL simulation and the right panel is the NOPLACE simulation.

Figure 11. Vertical cross section of the average water vapor mixing ratio Q (g kg^{-1}) and V wind (m s^{-1}) at 19N latitude during the1997 onset. The left panel is the CONTROL simulation and the right panel is the NOPLACE simulation.

Figure 12. Average latent heat flux (w m^{-2}) simulated during the 1997 onset. The left panel is the CONTROL simulation and the right panel is the NOPLACE simulation.

Figure 13. Vertical cross section of the average water vapor mixing ratio Q (g kg^{-1}) and U wind (m s^{-1}) at 105 E longitude during the1997 onset. The left panel is the CONTROL simulation and the right panel is the NOPLACE simulation.

Figure 14. Average sensible heat flux (w m^{-2}) simulated during the 1998 onset. The left panel is the CONTROL simulation and the right panel is the NOPLACE simulation.

Figure 15. Vertical cross section of the average water vapor mixing ratio Q (g kg^{-1}) and U wind (m s^{-1}) at 105 E longitude during the1998 onset. The left panel is the CONTROL simulation and the right panel is the NOPLACE simulation.

Figure 16. Sea surface temperature (SST) at a) the start (5/15/97) of the 1997 simulation and b) averaged over the entire 1997 simulation period. c) SST at the start (5/15/98) of 1998 simulation and d) averaged over the entire 1998 simulation period.

References

Betts, A. K., A new convective adjustment scheme. I: observations and theoretical basis. *Quart. J. Roy. Meteor. Soc.,* 112, 677-692. 1986.

Barnett, T. P., L. Dumenil, U. Schlese, and E. Roechner, The effect of Eurasian snow cover on regional and global climate variations. *J. Atmos. Sci.,* 46, 661-685. 1989.

Bosilovich, M. G, and W.-Y. Sun, Numerical simulation of the 1993 midwestern flood: Land-atmosphere interactions. *J. Climate*. 12, 1490-1505. 1999.

Bradley, E. F., P. A. Coppin, and J. S. Godfrey, Measurements of sensible and latent heat flux in the western tropical Pacific Ocean. *J. Geophys. Res.*, 96, 3375-3389. 1991.

Chen, T. and Coauthors, Cabauw experimental results from the project for intercomparison of land-surface parameterization schemes. *J. Climate*, 10, 1194-1215. 1997.

Ding, Y. H., Summer monsoon rainfalls in China. *J. Meteor. Soc. Japan*, 70, 373-396. 1992.

Ding, Y. H., The short-range fluctuations of monsoons and their association with the Meiyu weather events in China. Monsoons over China, Kluwere Acad. Pub., 174-230. 1994.

Dudhia, J., A numerical study of convection observed during the winter monsoon experiment using a mesoscale two-dimensional model. *J. Atmos. Sci.,* 46, 3077-3107. 1989.

Dudhia, J., A nonhydrostatic version of the Penn State/NCAR mesoscale model: validation of an Atlantic cyclone and cold front. *Mon. Wea. Rev.,* 121, 1493-1513, 1993.

Grell, G. A., J. Dudhia, and D. R. Stauffer, A description of the fifth-generation Penn State/NCAR mesoscale model (MM5), *Tech. Note, NCAR/TN-398+STR,* 138pp., NCAR, 1994.

He, Y. H., C, H. Guan, Z. J. Gan, Heat oscillation in the upper ocean of the South China Sea. *Acta Ocenologica Sinica*, 11, 375-388. 1992.

Holton, J. R., A introduction to dynamic meteorology. Academic Press, NY. 319pp. 1972.

Huffman, G. J. and Coauthors, The Global Precipitation Climatology Project (GPCP) combined precipitation dataset. *Bull. Amer. Meteor. Soc.,* 78. 5-20. 1997.

Johnson, R. H. and P. E. Ciesielski, Characteristics of the 1998 summer monsoon onset over the Northern South China Sea. *J. Meteor. Soc. Japan.* (submitted). 2003.

Kummerow, C., Y. Hong, W. S. Olson, S. Yang, R. F. Adler, J. McCollum, R. Ferraro, G. Petty, D.-B. Shin and T. T. Wilheit, The evolution of the Goddard Profiling Algorithm (GPROF) for rainfall estimation from passive microwave sensors. *J. Appl. Meteor.,* 40: 1801-1820. 2001.

Lau, K.-M. and S. Yang, Climatology and Interannual variability of the Southeast Asian summer monsoon. *Adv. Atmos. Sci.*, **14**, 141-162. 1997.

Lau , K.-M and S. Shen, Biennial oscillation associated with the East Asia summer monsoon and tropical sea surface temperature. East Asian and Western Pacific Meteorology and Climate, II, W. J. Kyle and C. P. Chang Eds., *World Scientific Publication Co.,* 65-72. 1992.

Lau, K.-M. and X. Li, Evolution of the large scale circulation, cloud structure and regional water cycle associated with the South China Sea monsoon during May-June, 1998. *J. Meteor. Soc. Japan,* (submitted). 2003.

Lau, K.-M., H. –T. Wu, and S. Yang, Hydrologic processes associated with the first transition of the Asian summer monsoon: A pilot satellite study. *Bull. Amer. Meteor. Soc.*, 79, 1871-1882. 1998.

Liang, X.-Z. and W.-C. Wang, Associations between China monsoon rainfall and tropospheric jets. *Quart. J. Roy. Meteor. Soc.*, 124, 2597-2623. 1998.

Lynn, B. H., D. R. Stauffer, P. J. Wetzel, W.-K. Tao, P. Alpert, N. Perlin, R. D. Baker, R. Munoz, A. Boone and Yiqin Jia, Improved simulation of Florida summer convection using the PLACE land model and a 1.5-order turbulence parameterization coupled to the Penn State/NCAR Mesoscale Model, Mon. Wea. Rev., 129, 1441-1461. 2001.

Meehl, G. A., The annual cycle and relationship to interannual variability in the tropical Pacific and Indian Ocean regions. *Mon. Wea. Rev.*, 115, 27-50. 1987.

Meeson, B. W., and Coauthors, ISLSCP initiative I – Global data sets for land-atmosphere models, 1987-1988. Volumes 1-5, Published on CD by NASA (USA_NASA_GDDAC_ISLSCP_001-USA_NASA__GDDAC_ISLSC_001). 1995.

Qian, J. –H., W.-K. Tao, and K.-M. Lau, Mei-yu Moisture processes. *Mon. Wea. Rev.,* (submitted). 2003.

Samel, A. N., S. Wang, and W.-C. Wang, A comparison between observed and GCM-simulated summer monsoon characteristics over China. *J. Climate*, 8, 1690-1696. 1995.

Sperber, K. R., S. Hammed, G. L. Potter, and J. S. Boyle, Simulation of the northern summer monsoon in the ECMWF model: sensitivity to horizontal resolution. *Mon. Wea. Rev.*, 122, 2461-2481. 1994.

Tao, S. and L. Chen, A review of recent research on the east Asian summer monsoon in China. Monsoon Meteorology, C. –P. Chang and T. N. Krishnamurti, Eds., Oxford University Press, 60-92. 1987.

Tao, W. –K., C. S. Chen, Y. Jia, D. Baker, S. Lang, P. Wetzel, and K. –M. Lau, A study of heavy precipitation events in Taiwan during 10-13 August, 1994, Part II: Mesoscale model simulations. *J. Meteor. Soc. Japan* (submitted). 2003.

Wang, W.-C., W. Gong, and H. Wei, A regional model simulation of 1991 severe precipitation event over the Yangtze-Huai river valley. Part I: precipitation and circulation statistics. *J. Climate*, 13, 74-92. 2000.

Wang, Y., W.-K. Tao, and J. Simpson, The impact of ocean surface fluxes on a TOGA COARE convective system. *Mon. Wea. Rev.*, 124, 2753-2763. 1996.

Wetzel, P. J. and A. Boone, A parameterization for Land-Atmosphere-Cloud Exchange (PLACE): Documentation and testing of a detailed process model of the partly cloudy boundary layer over heterogeneous land. J. Climate, 8, 1810-1837. 1995.

Young, G. S., D. V. Ledvina, and C. W. Fairall, Influence of precipitating convection on the surface energy budget observed during a tropical ocean global atmosphere pilot cruise in the tropical western pacific ocean. *J. Geophy. Res.*, 97, 9595-9603. 1992.

Zhang, D.-L. and R. A. Anthes, A high-resolution model of the planetary boundary layer sensitivity tests and comparisons with SESAME-79 data. *J Appl. Meteor.*, 21, 1594-1609, 1982.

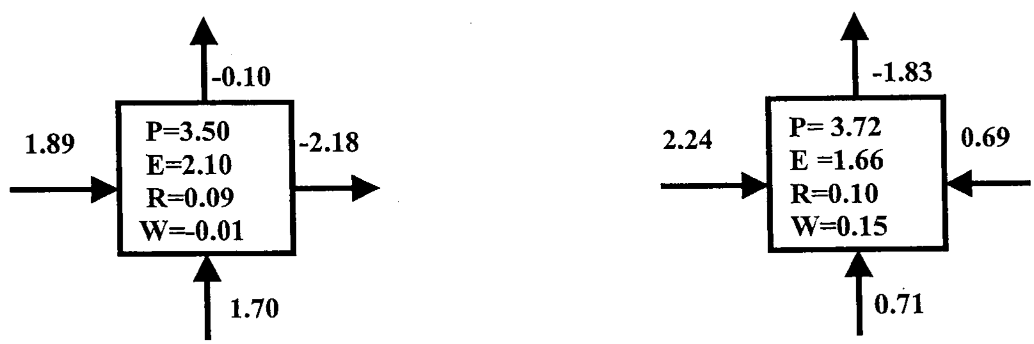

Year 1997

Year 1998

Fig. 8

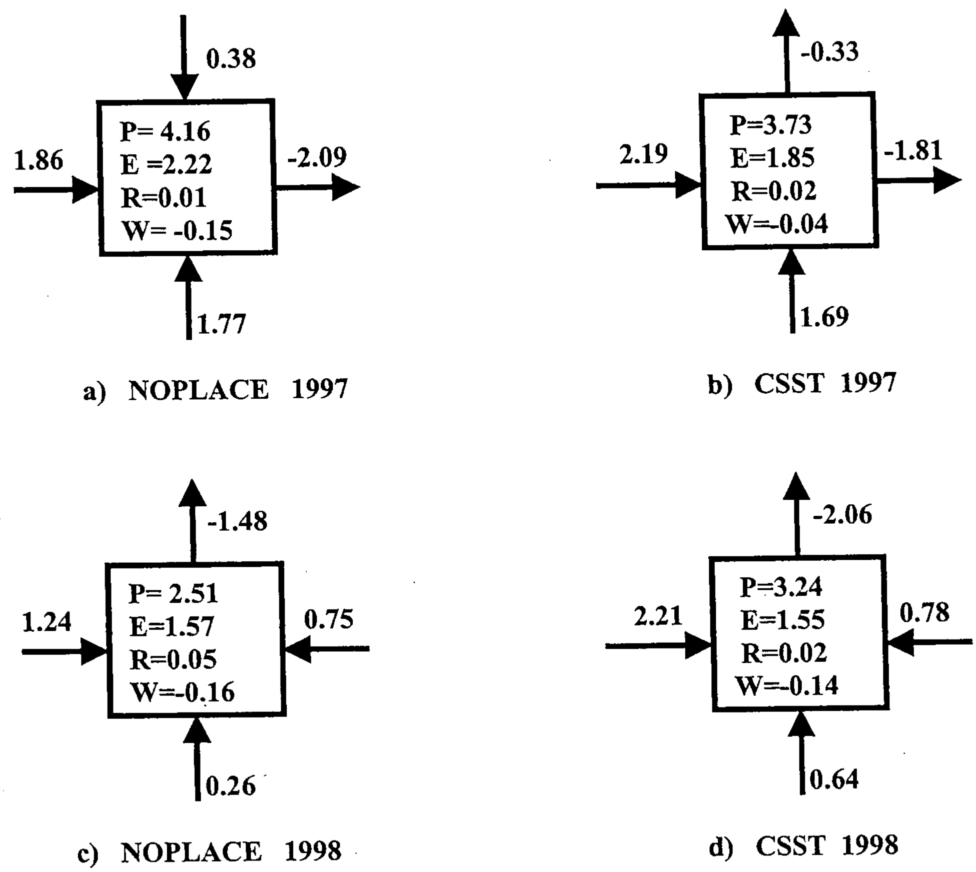
0.38
1.86
P= 4.16
E =2.22
R=0.01
W= -0.15
-2.09
1.77
a) NOPLACE 1997
-0.33
2.19
P=3.73
E=1.85
R=0.02
W=-0.04
-1.81
1.69
b) CSST 1997
-1.48
1.24
P= 2.51
E=1.57
R=0.05
W=-0.16
0.75
0.26
c) NOPLACE 1998
-2.06
2.21
P=3.24
E=1.55
R=0.02
W=-0.14
0.78
0.64
d) CSST 1998

Fig. 9

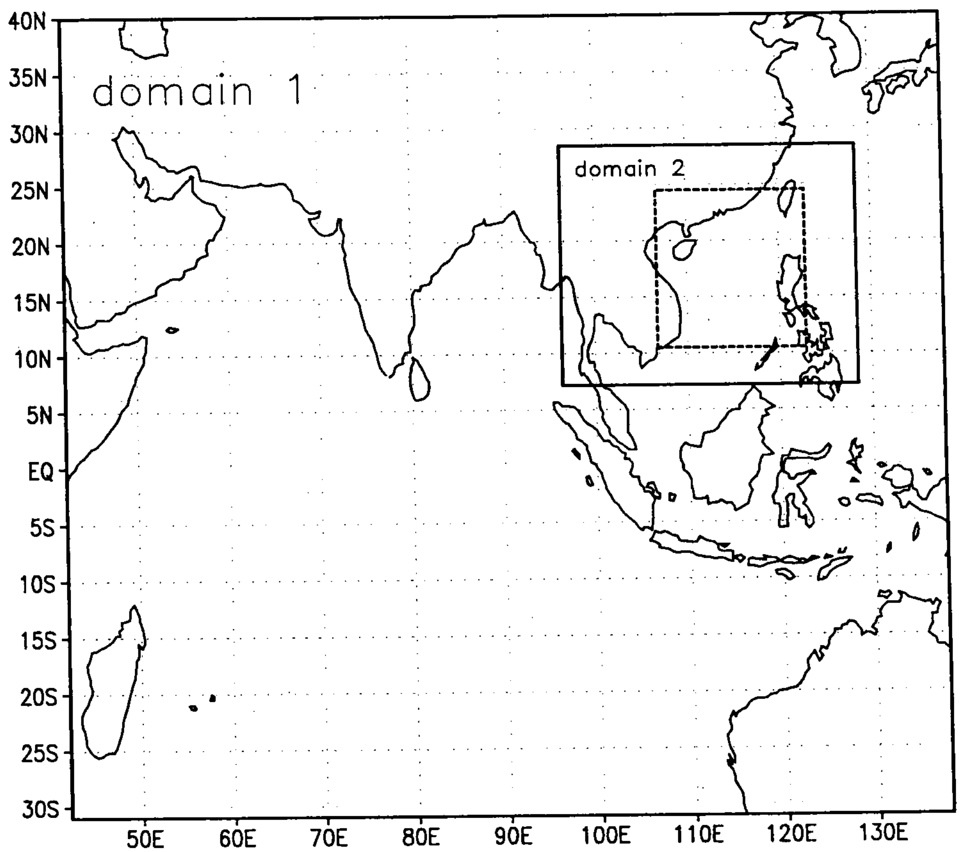

domain 1
domain 2
40N
35N
30N
25N
20N
15N
10N
5N
EQ
5S
10S
15S
20S
25S
30S
50E
60E
70E
80E
90E
100E
110E
120E
130E

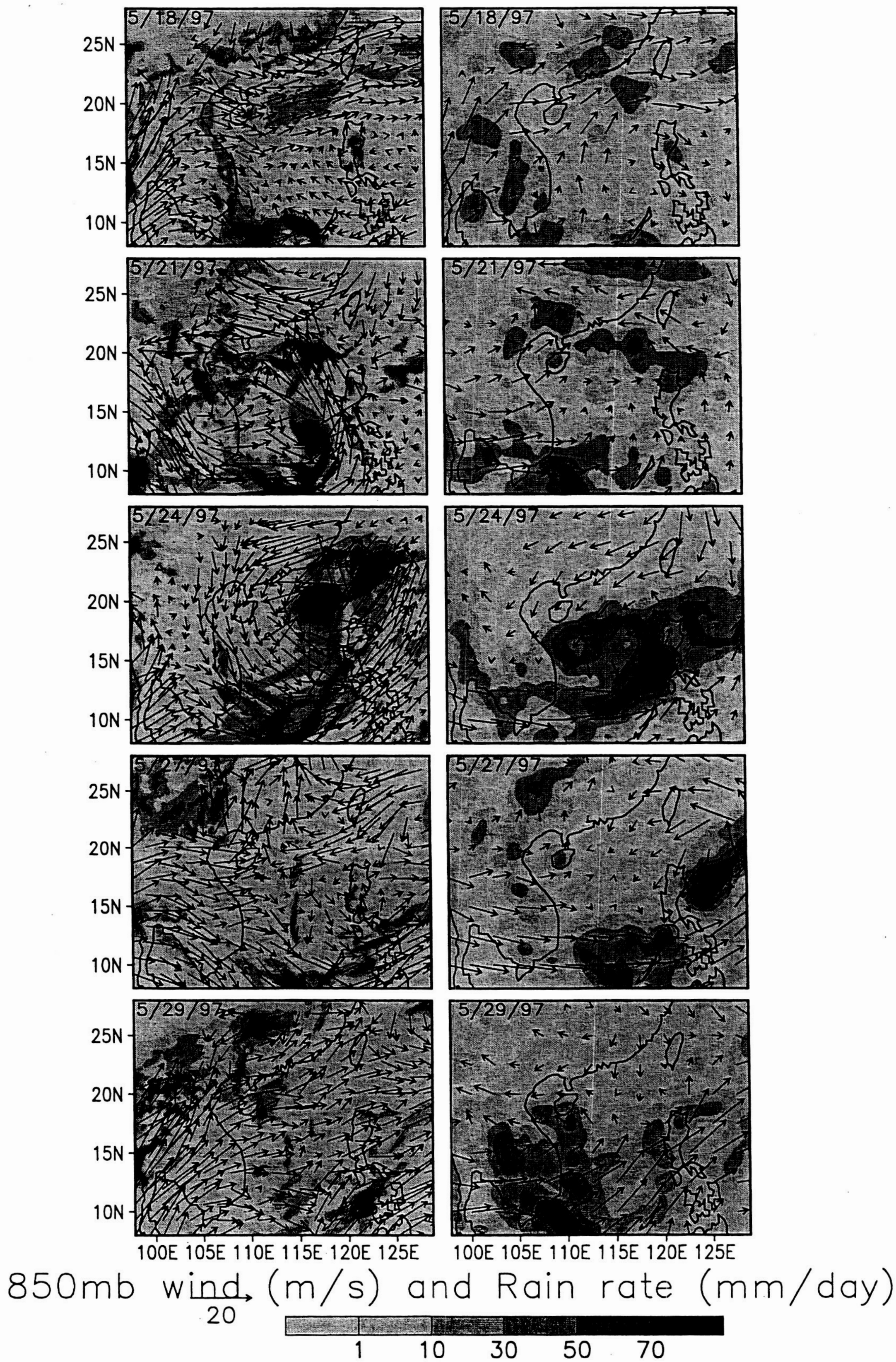
5/18/97
5/18/97
5/21/97
5/21/97
5/24/97
5/24/97
5/27/97
5/27/97
5/29/97
5/29/97
25N
20N
15N
10N
100E 105E 110E 115E 120E 125E
100E 105E 110E 115E 120E 125E
850mb wind (m/s) and Rain rate (mm/day)
20
1
10
30
50
70

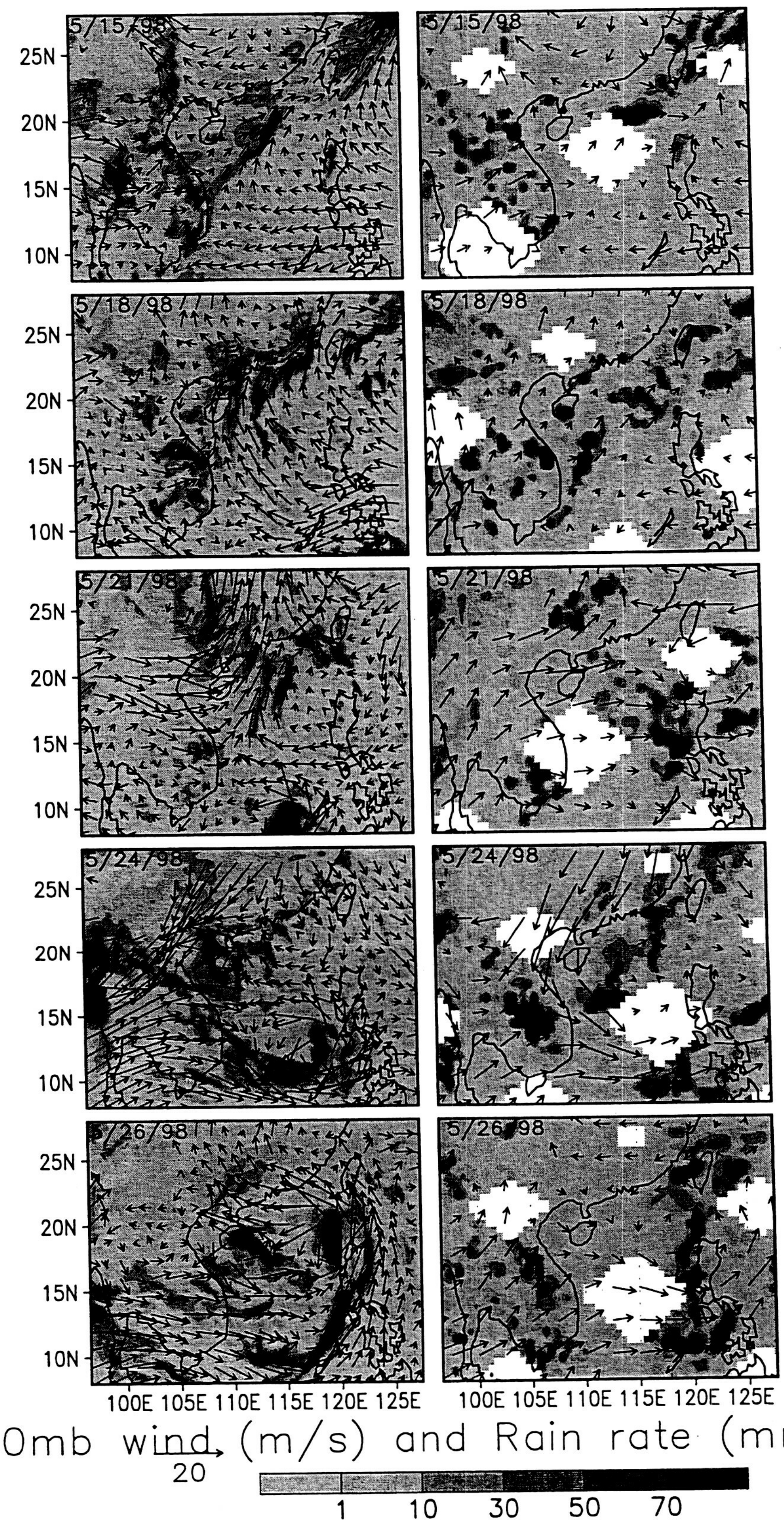

850mb wind (m/s) and Rain rate (mm/day)

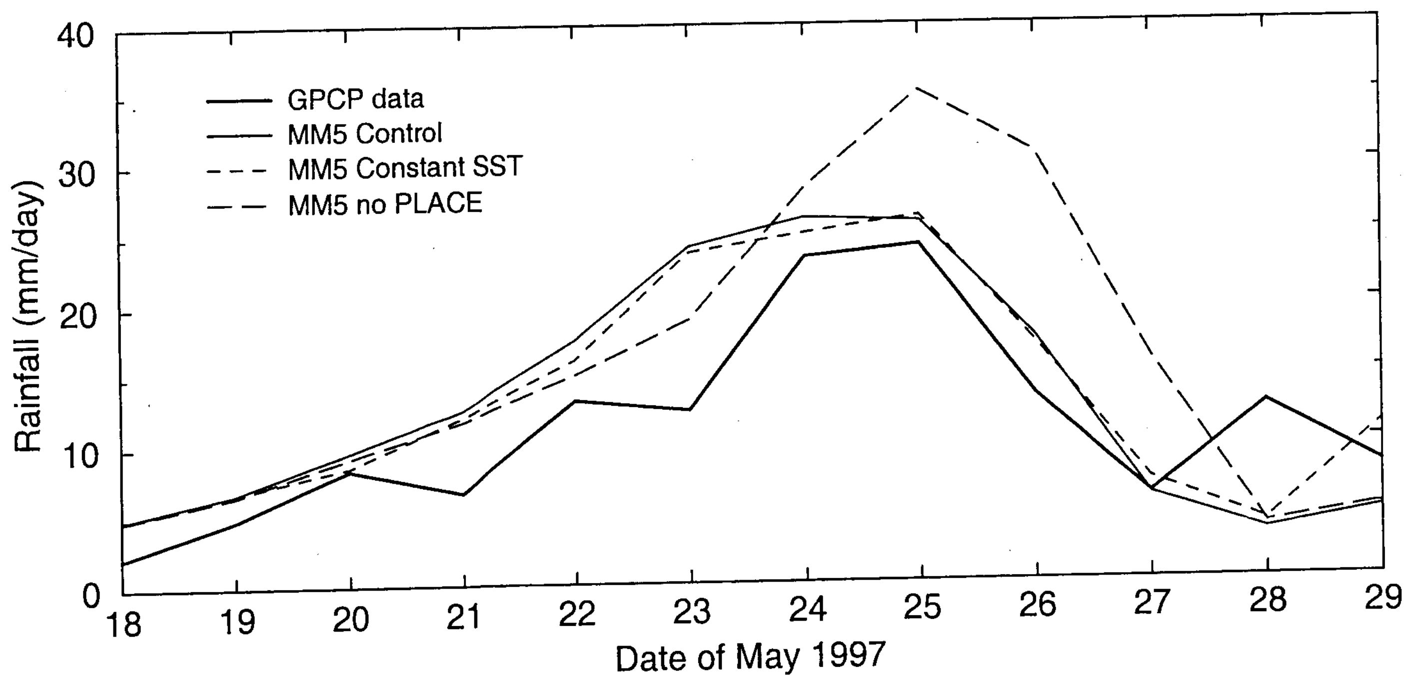

Rainfall (mm/day)
0
10
20
30
40
18
19
20
21
22
23
24
25
26
27
28
29
Date of May 1997
GPCP data
MM5 Control
MM5 Constant SST
MM5 no PLACE

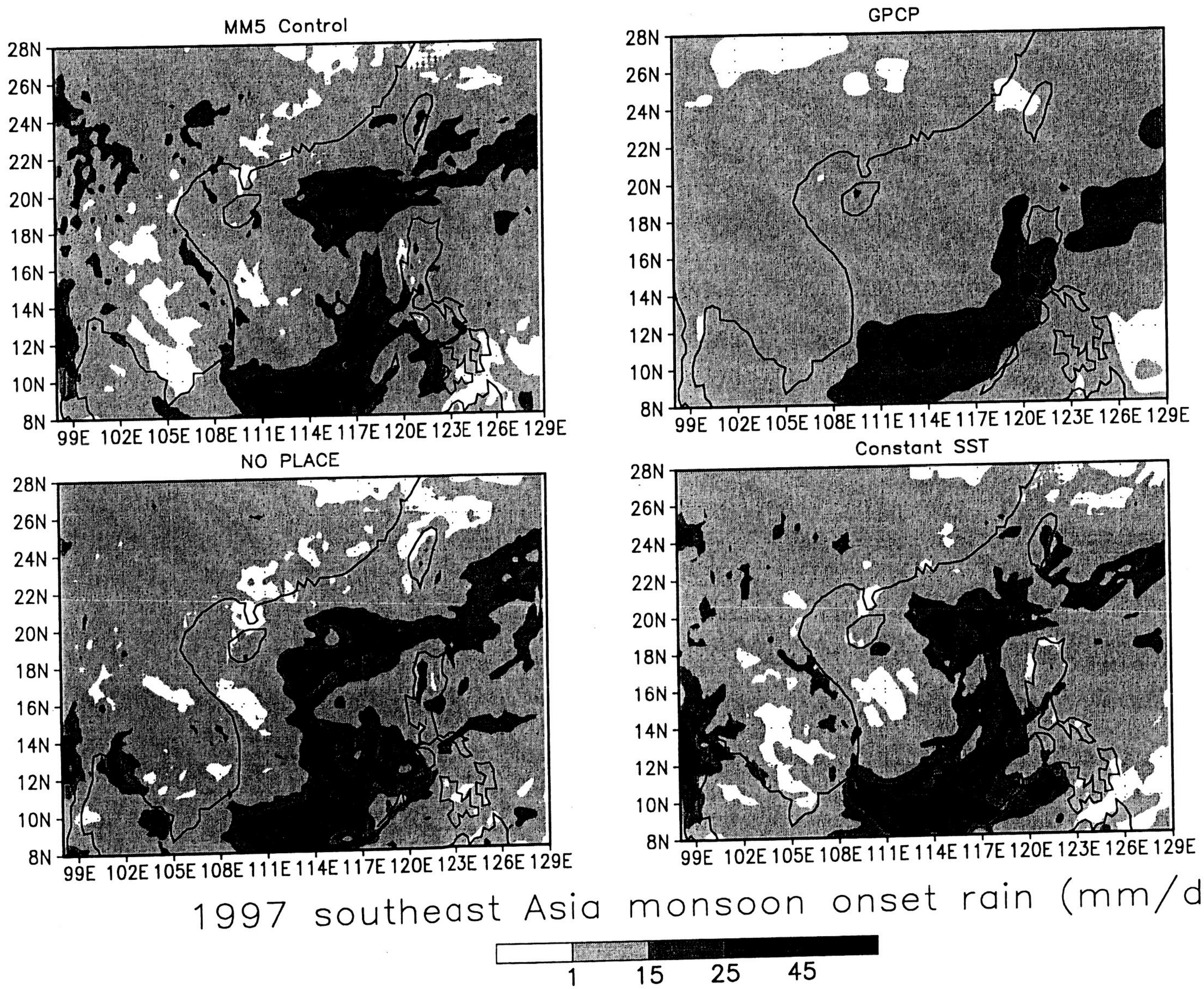

1997 southeast Asia monsoon onset rain (mm/day)

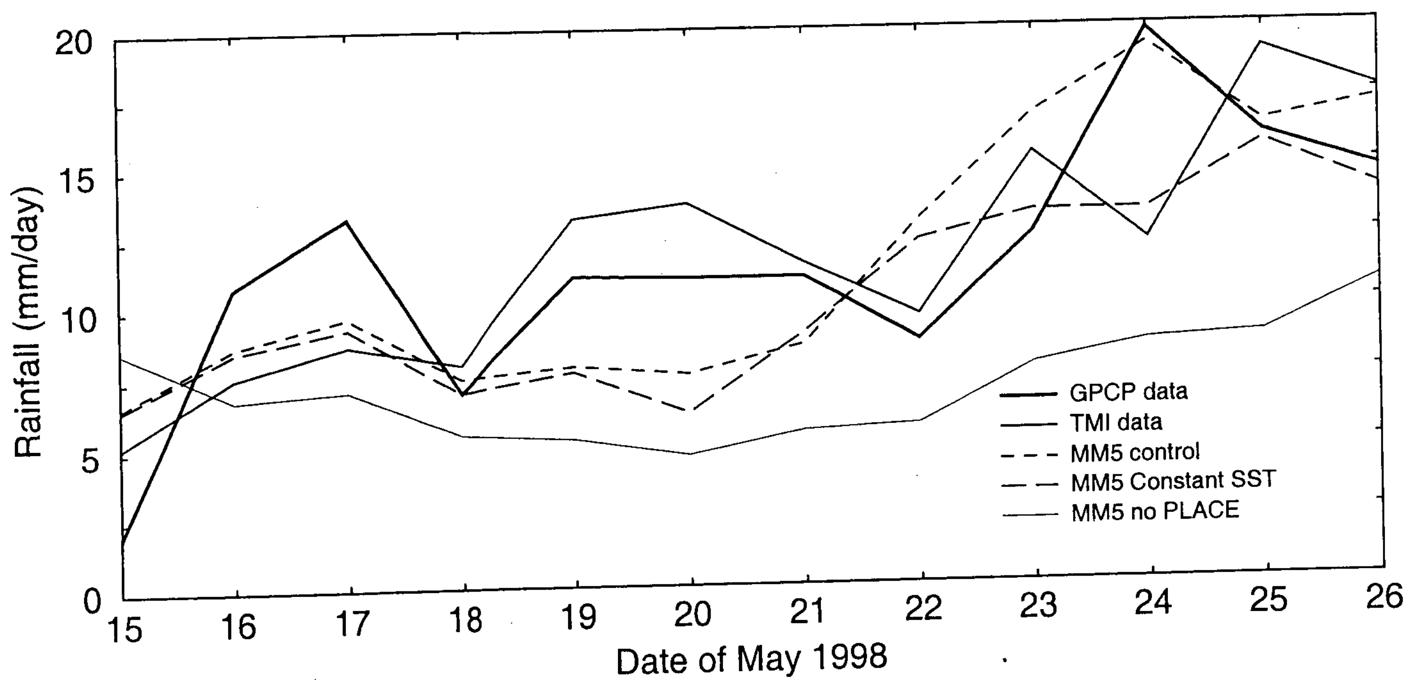

Rainfall (mm/day)
0
5
10
15
20
15
16
17
18
19
20
21
22
23
24
25
26
Date of May 1998
GPCP data
TMI data
MM5 control
MM5 Constant SST
MM5 no PLACE

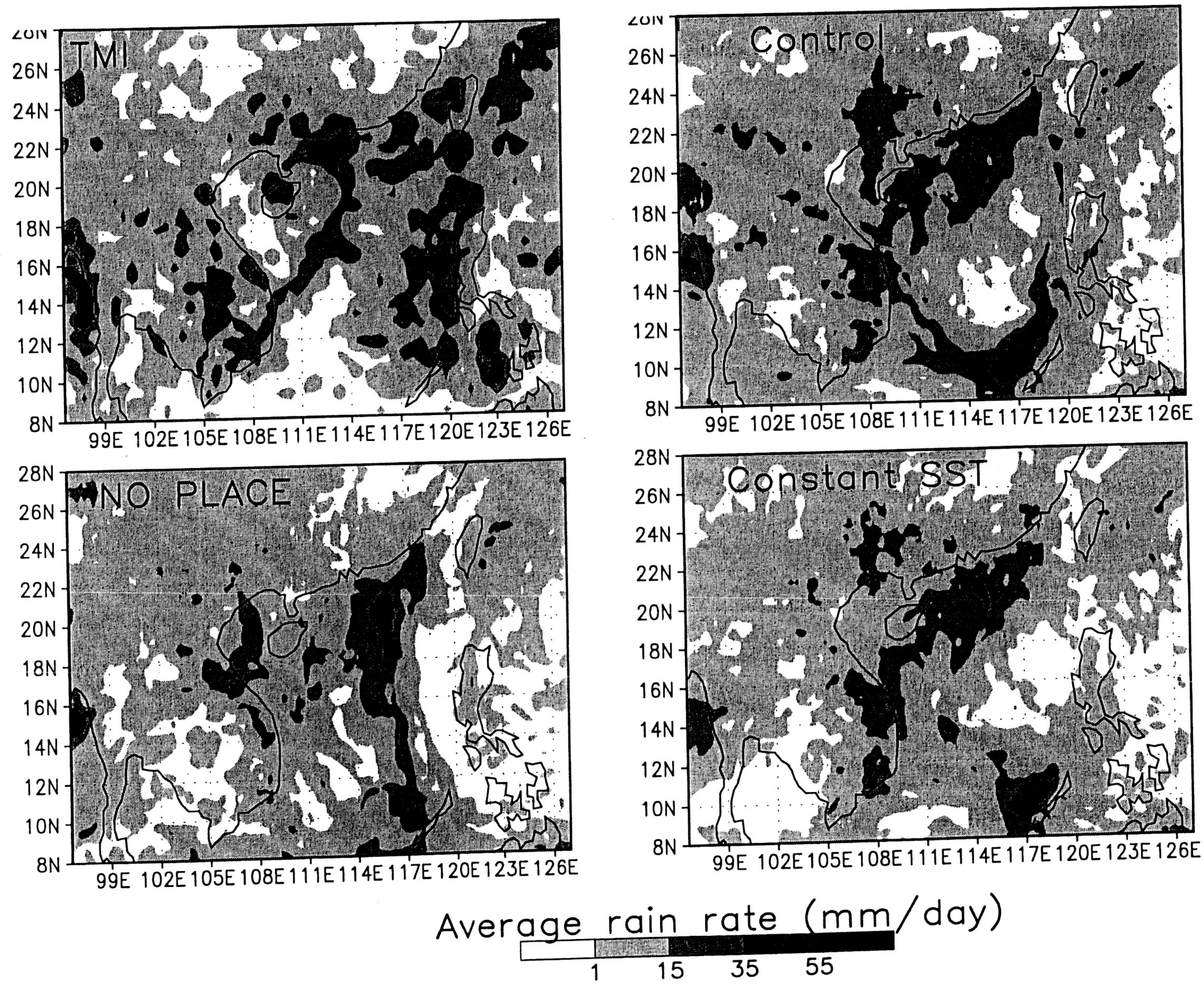
TMI
Control
NO PLACE
Constant SST
28N 26N 24N 22N 20N 18N 16N 14N 12N 10N 8N
99E 102E 105E 108E 111E 114E 117E 120E 123E 126E
Average rain rate (mm/day)
1 15 35 55

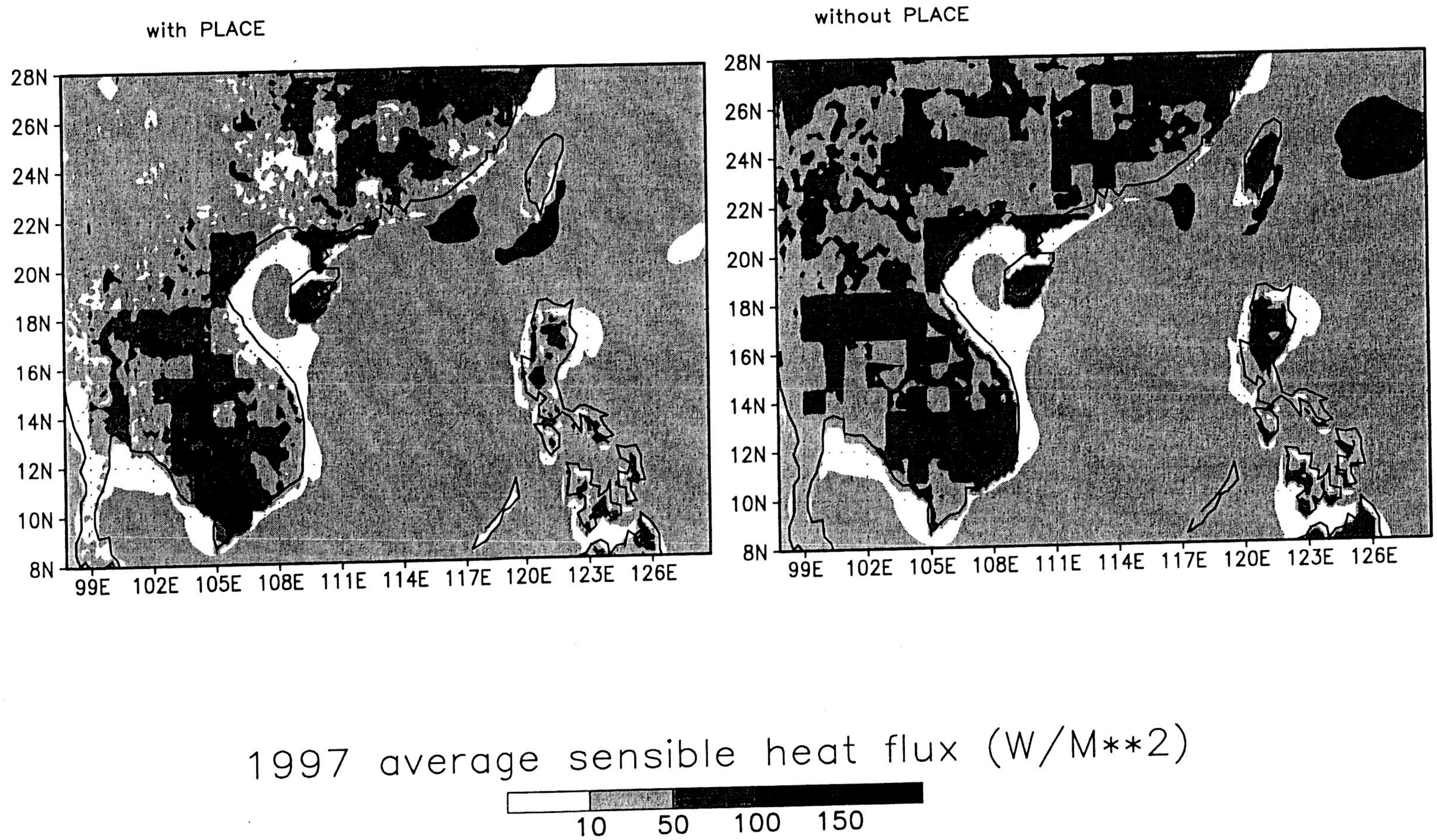

1997 average sensible heat flux (W/M**2)

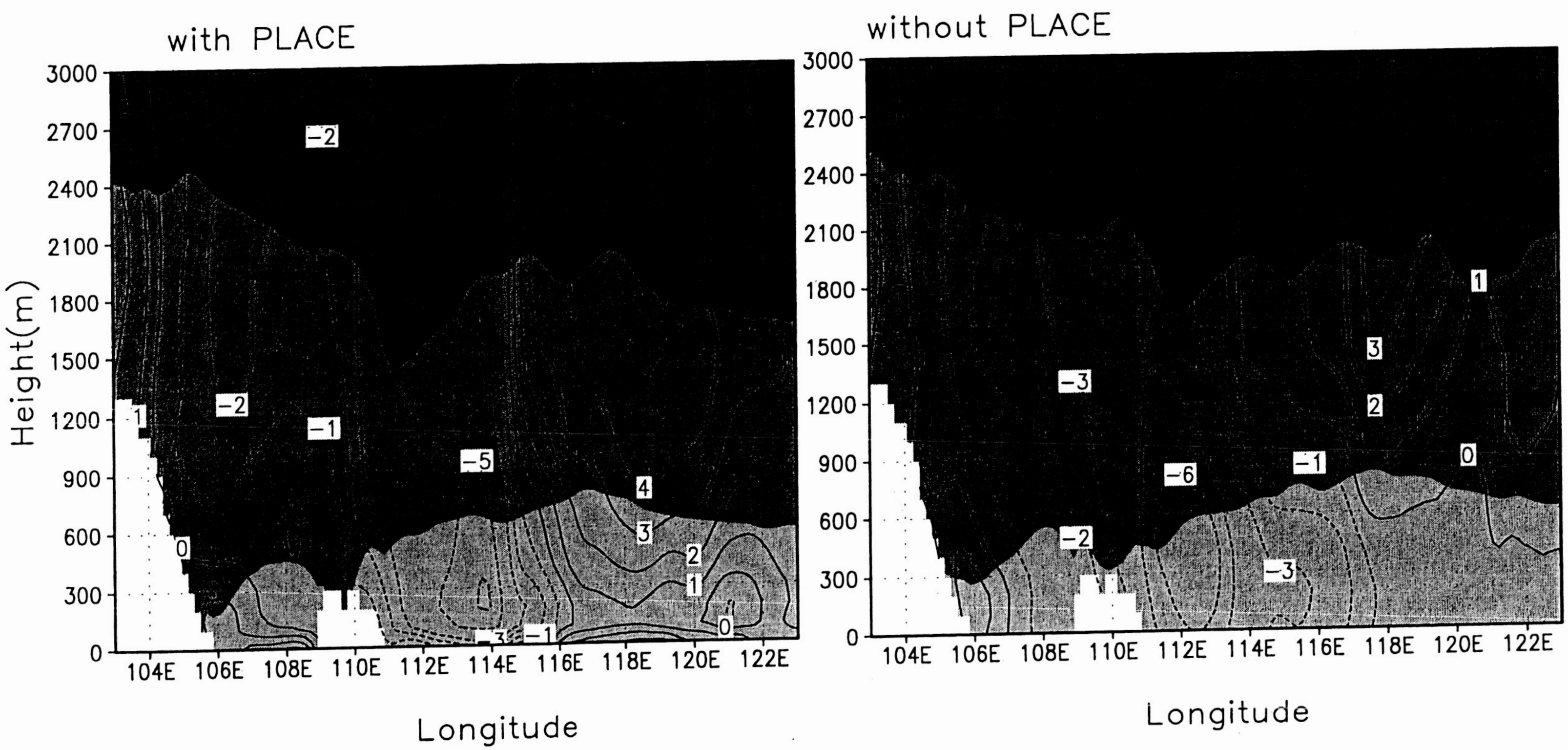

Averaged Q(g/kg) and V(m/s) at 19N cross section(1997)

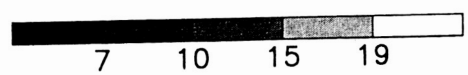

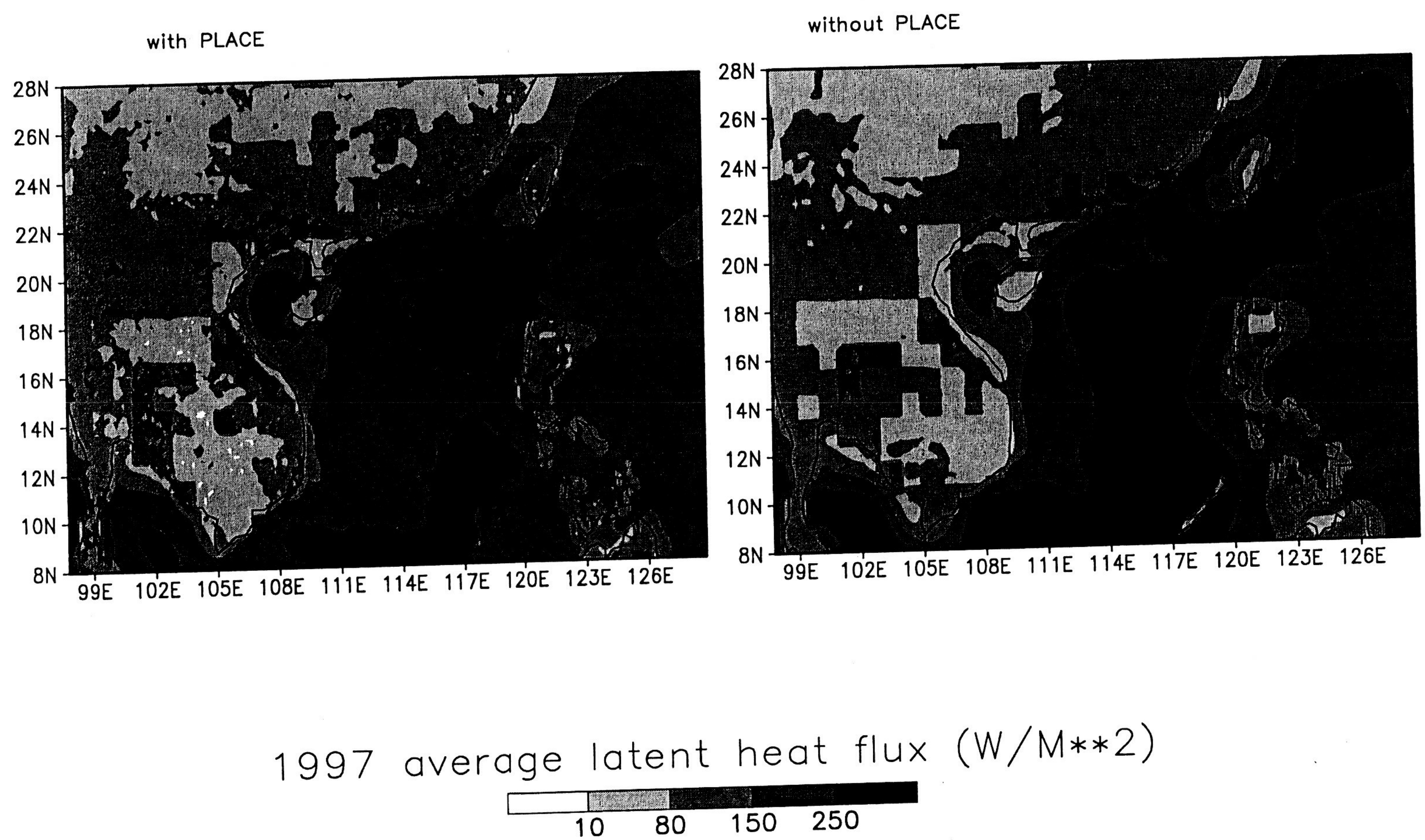

1997 average latent heat flux (W/M**2)

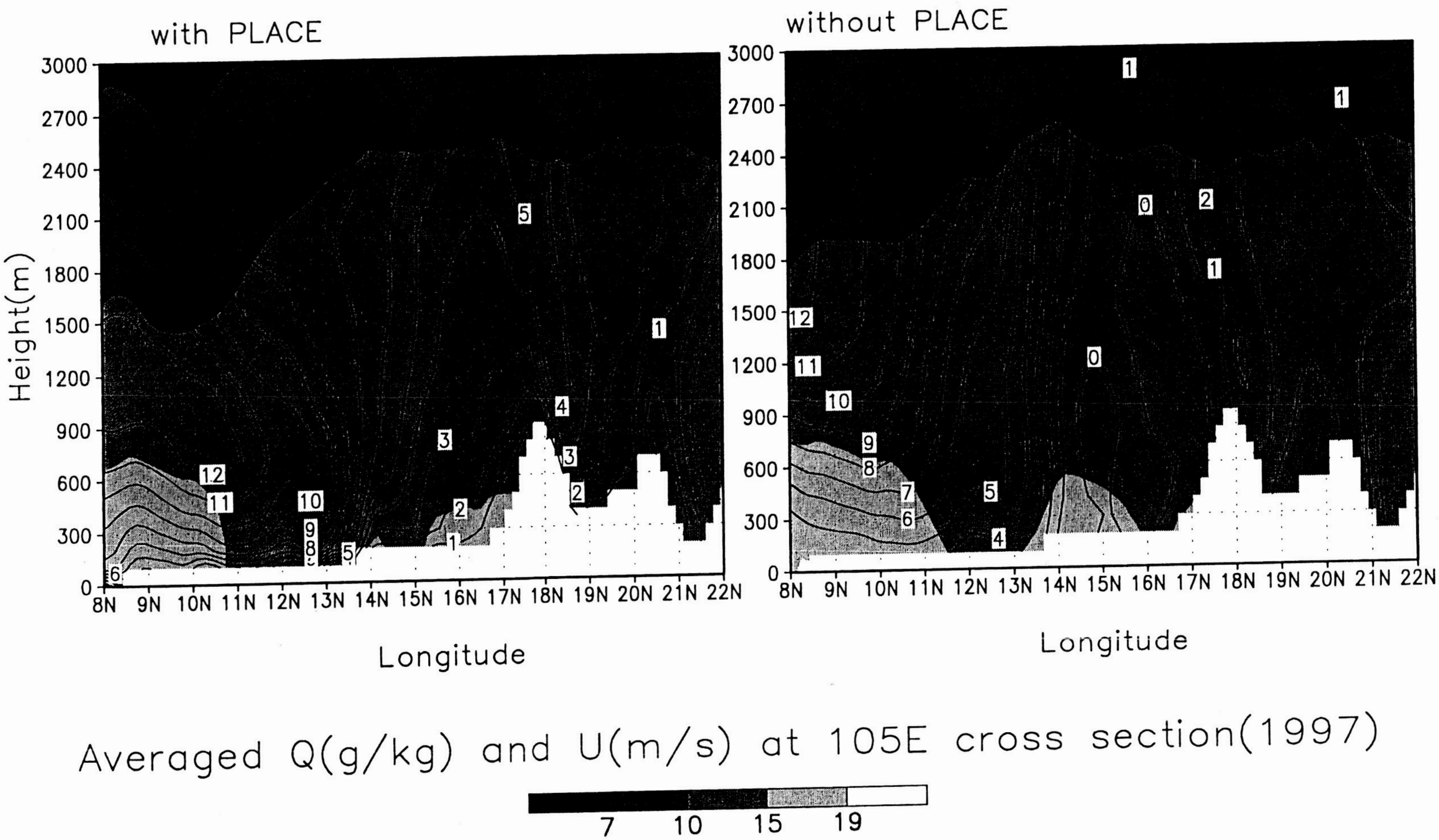

Averaged Q(g/kg) and U(m/s) at 105E cross section(1997)

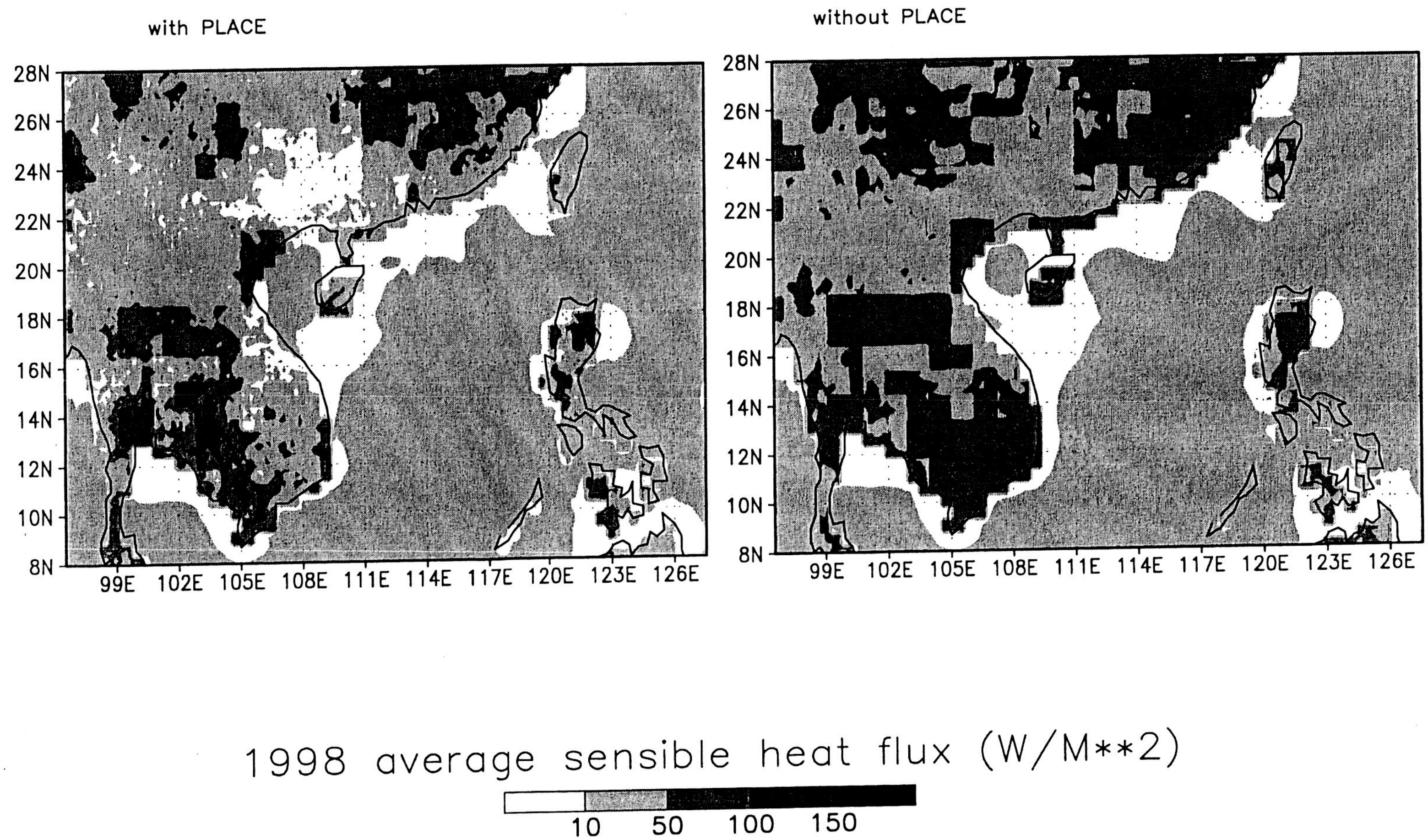

1998 average sensible heat flux (W/M**2)

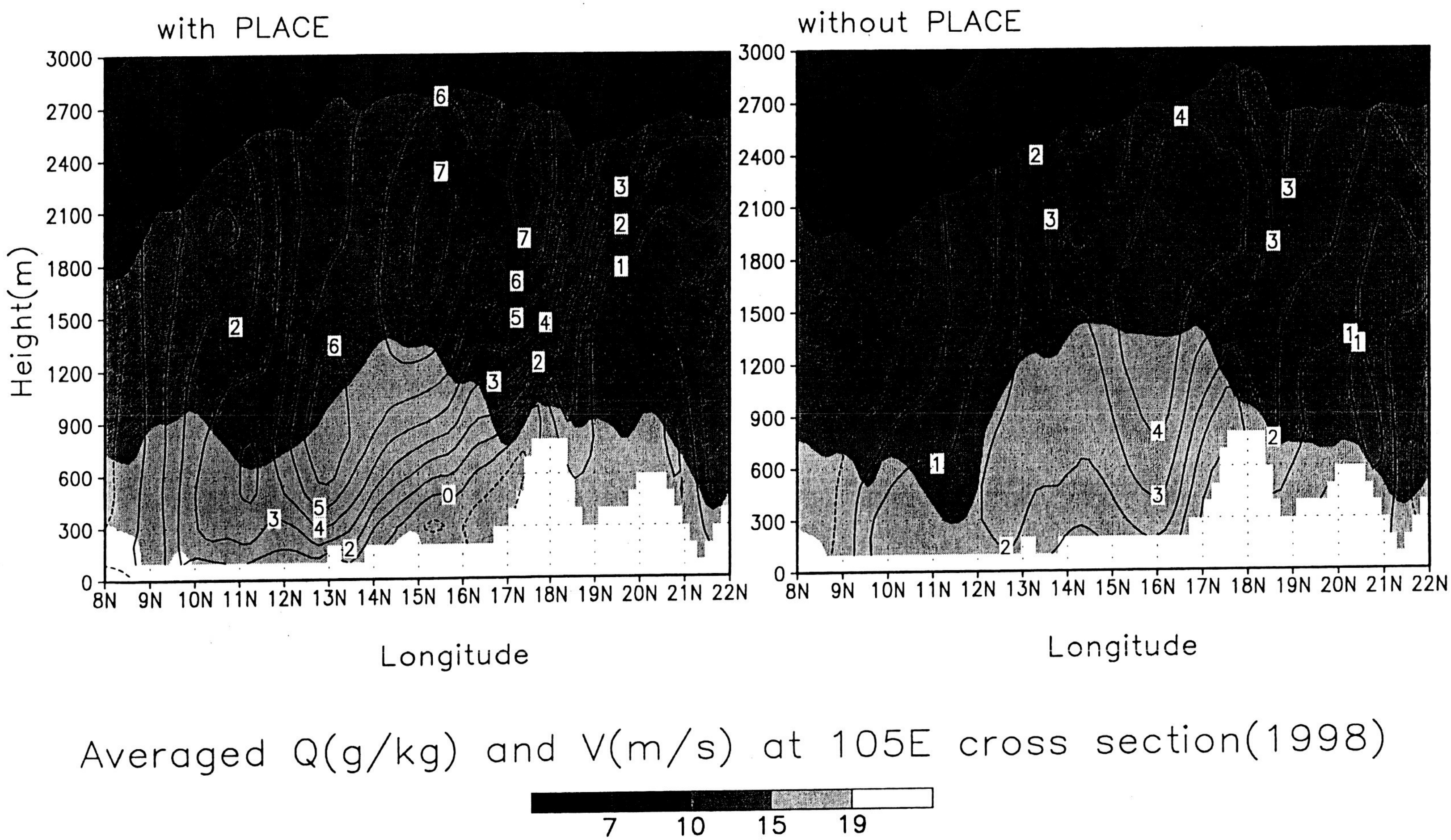

Averaged Q(g/kg) and V(m/s) at 105E cross section(1998)

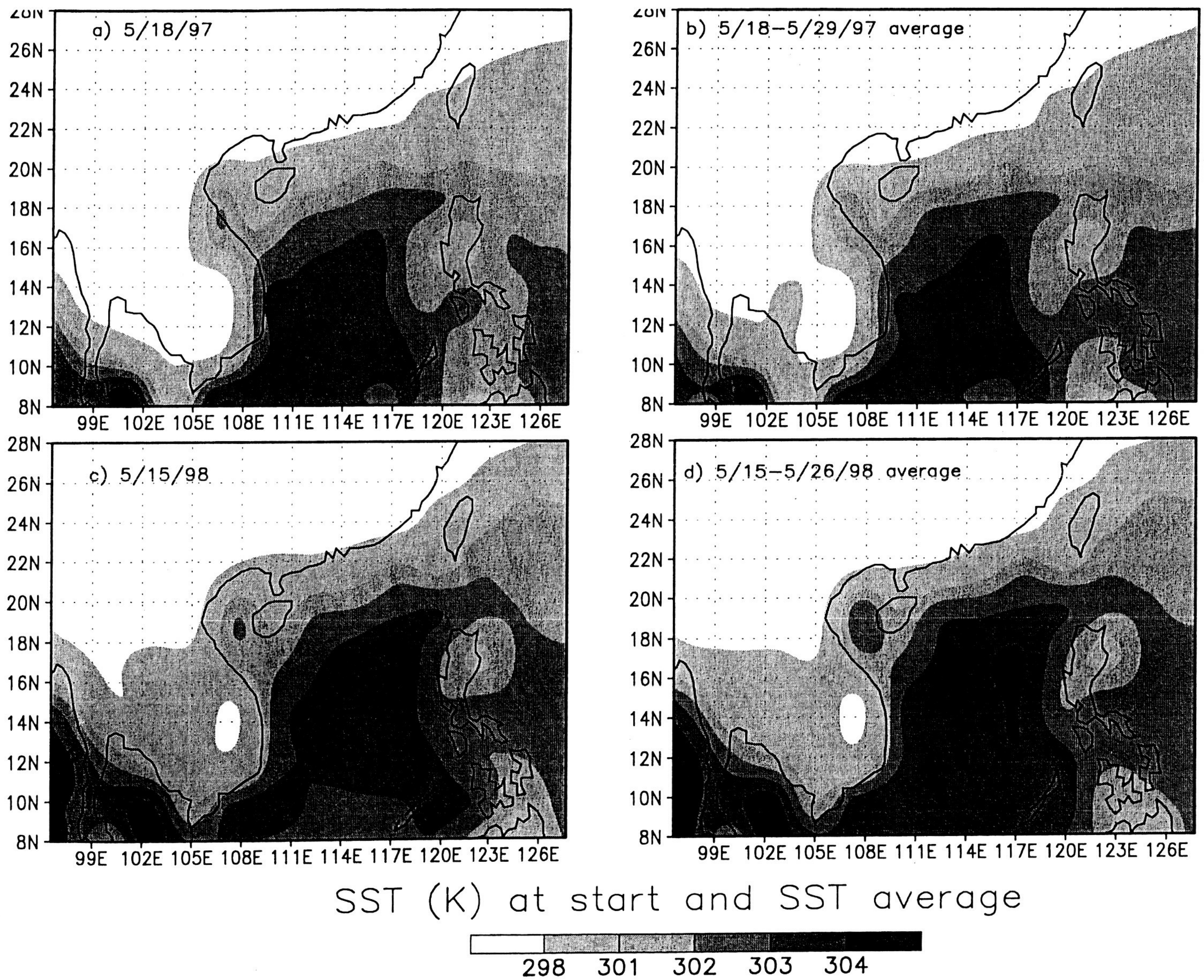
a) 5/18/97
b) 5/18–5/29/97 average
c) 5/15/98
d) 5/15–5/26/98 average
28N 26N 24N 22N 20N 18N 16N 14N 12N 10N 8N
99E 102E 105E 108E 111E 114E 117E 120E 123E 126E
SST (K) at start and SST average
298 301 302 303 304